Available online at www.sciencedirect.com
ScienceDirect
Nuclear Instruments and Methods in Physics Research B 266 (2008) 1971–1978
NIM B
Beam Interactions with Materials & Atoms
www.elsevier.com/locate/nimb

Implantation effects of low energy H and D ions in germanium at −120 °C and room temperature

Nicholas Desrosiers [a], Alexandre Giguère [a], Bernard Terreault [a,*], Martin Chicoine [b], François Schiettekatte [b]

[a] INRS-EMT, Université du Québec, 1650 Boul. Lionel-Boulet, Varennes, Québec, Canada J3X 1S2
[b] Département de physique, Université de Montréal, C.P. 6128, succ. Centre-Ville, Montréal, Québec, Canada H3C 3J7

Received 31 January 2008; received in revised form 7 March 2008
Available online 18 March 2008

Abstract

Germanium was implanted with 5 keV H and D ions at −120 °C or room temperature and thermally annealed in several steps. The samples were analysed at various stages by atomic force microscopy, ion channeling and Raman spectroscopy of Ge-H/D local vibration modes. The results are discussed in comparison with those in the well studied silicon. In general, the evolution of the different types of defects, in germanium at a given temperature, tends to be similar to that of the corresponding defects in silicon at 100–300 °C higher temperature. However, the behaviour of the defects detected by ion channeling (interstitials, lattice distortions) often appears unrelated to the chemical evolution measured by Raman scattering and to the temperature and isotope dependence of blistering.

PACS: 61.72.Uf; 61.82.Fk; 85.40.–e

Keywords: Ion implantation; Radiation defects; Germanium; Hydrogen isotopes; Blistering

1. Introduction

Because of its high carrier mobility and small band gap, germanium is already used as a versatile photon detector and it is envisaged for niche applications in electronic circuitry. Behaviour under ion irradiation is a crucial technological property of semiconductors: Besides its obvious relevance when used as a γ-ray detector or in circuitry exposed to radiation, irradiation behaviour is also important because ion etching and ion implantation are extensively utilized in semiconductor processing. One such process of rapidly growing use is ion-cutting and layer transfer [1], which is based on hydrogen ion implantation followed by layer bonding and thermal annealing. Developed for the purpose of silicon-on-insulator fabrication [1] and exhaustively studied in that context in the last decade [2], this process has been extended to several other materials, including germanium [3–7]. However, in the case of Ge, there are still some contradictions and ambiguities in the literature. For instance, there is disagreement on the threshold dose for blistering, surprisingly reported as higher ($\sim 5 \times 10^{16}$ H/cm^2) at 80 keV [6] than at 100 keV ($\sim 4 \times 10^{16}$ H/cm^2) [4]. Perhaps more significant in terms of the physics, the phenomenological activation energy is given as 1.0 eV in [3] and 1.8 eV in [4]. In addition, a recent report [7] has shown the important effect of the implantation temperature (in the range between room temperature and 150 °C) on the defect structures observed by transmission electron microscopy.

In the present work, the effects of H ion implantation in Ge at low temperature (LT = −120 °C) and at room temperatures (RT) are investigated, using atomic force microscopy, ion channeling and Raman spectroscopy of Ge-H local vibration modes. The results show again the importance of the implantation temperature, which suggests that

* Corresponding author. Tel.: +1 450 929 8111; fax: +1 450 929 8102.
E-mail address: terreault@emt.inrs.ca (B. Terreault).

0168-583X/$ - see front matter © 2008 Elsevier B.V. All rights reserved.
doi:10.1016/j.nimb.2008.03.081

the cited discrepancies may be due to a loose control of that temperature in some of the previous investigations. Further insight into radiation effects in Ge was also sought by comparing H and D ion implantation, in view of the giant isotope effect observed in Si [8]. Another difference with earlier work is the use of low energy ions (5 keV/atom), having a mean range of only 54 nm [9], which will allow comparably thin transferred layers to be obtained for the fabrication of germanium-on-insulator or other devices. Finally, similarities and differences with the better known case of silicon [2] are pointed out and their significance discussed.

2. Experimental details

Commercially available, electronic grade, single crystalline 2 in. wafers with (0 0 1) orientation and a resistivity >35 Ω-cm were used. They were cleaved into 1 cm^2 pieces and implanted with 10 keV H_2^+ or D_2^+ ions to doses in the range of (1–8) × 10^{16} atom/cm^2, using an ion implanter having a base pressure <10^{-7} mbar. (All doses will be given in terms of atoms, not ions and the energy per atom assumed to be 5 keV). The mean scanned current was ≈1 μA, resulting in negligible sample heating. Some samples were implanted without active cooling, whereas others were maintained at −120 ± 5 °C by fixing them at the tip of an electrically insulated copper rod whose other end was dipped in liquid nitrogen outside the vacuum chamber. The sample temperature was measured by a thermocouple inserted in the target holder right behind the target.

Afterwards, some samples were cut again into four pieces and a subset subjected to rapid thermal annealing (RTA) for 30 s at 600 °C under a nitrogen flow. The surface morphology of the samples was observed before and after annealing by atomic force microscopy (AFM) using a Nanoscope IIIa from Digital Instruments. Statistical analysis of the images was performed using the WSxM software package [10].

Other samples were ramped up to 200, 300 or 400 °C in a vacuum furnace and annealed for 30 min, prior to their analysis by Rutherford backscattering of ^4He ions in the axial channeling mode (RBS/C). This technique is sensitive to the presence of atoms in interstitial sites, either displaced lattice atoms or impurities and to lattice distortions. The beam energy was 2 MeV, its incidence angle 0 ± 0.1°, the current ~5 nA, the total charge 2 or 5 μC, the backscattering angle 170°, the detector solid angle 8.1 mSr, the detector resolution 20 keV (fwhm). Measurements were also carried out using either an unimplanted wafer (virgin) or with the beam off by several degrees from the crystal axis (random); the contrast between these two is a measure of the quality of the beam alignment.

Other samples were analysed by Raman scattering (RS) spectroscopy in the Ge-H (or Ge-D) stretch mode region. This allows the study of the evolution of those complexes that result from H/D passivation of the dangling bonds produced by the implantation process. In this case, the annealing protocol consisted of a slow ramp of 0.33 °C/s up to the target temperature, in air, at which point the samples were let to cool off immediately. The Raman spectrometer was a Renishaw 3000 operated at RT and having a resolution of 2 cm^{-1}; the exciting wavelength was 514 or 633 nm, at normal incidence, the spectrum acquisition time 500 s; several spectra were added in order to increase the signal/noise ratio and facilitate the subtraction of the luminescence background.

3. Results

3.1. Blistering phenomenology

Surface blistering is the most obvious effect observed and its dose threshold is an important parameter for its practical application in ion-cutting and layer transfer. For all doses of H or D ions equal to or larger than 2 × 10^{16} cm^{-2}, whether implanted −120 °C or room temperature, there is abundant blistering after annealing; Fig. 1 illustrates for instance the case of D implanted at −120 °C. In a finer investigation of the dose dependence at RT [11], it was found that abundant blistering (~70% surface coverage) suddenly appeared for (1.4 ± 0.1) × 10^{16} cm^{-2} of both H or D ions. This is definitely smaller than in Si at the same energy [8]; that observation is contrary to [6] but in agreement with [4]. In addition, Ge was found to start blistering following RT implantation, without any anneal, for H doses of 5 × 10^{16} H/cm^2 and more: see Fig. 2. However, it can be seen that the blisters are actually sparse for (5–6) × 10^{16} H/cm^2 and that the threshold for abundant blistering is closer to 7 × 10^{16} H/cm^2. No such RT blistering is observed for D ions or for LT implants. All this phenomenology is similar to that observed in Si [8,12], but with a shift as a function of the implantation temperature. For instance, the results for Ge blistering after annealing display no significant isotope dependence, a situation that obtains in Si only for implantation temperatures around 175 °C. The only isotope effect in Ge concerns blistering by implantation at RT without post-implant annealing, seen with H but not D. That RT blistering requires lower doses (~1/3) or implantation temperatures (~100 °C less) in Ge than in Si [12]. Another point is that, when H or D are implanted at RT in Si, blistering is no more observed for higher doses (> 4 × 10^{16} H/cm^2 or > 8 × 10^{16} D/cm^2, about twice the threshold doses), a phenomenon not observed in Ge at RT, but which disappears above 100 °C in Si. Thus, the Ge blistering behaviour under H/D irradiation appears in several ways similar to that of Si at implantation temperatures that are 100–300 °C higher, depending on the case.

3.2. Ion channeling

In Fig. 3 are shown the backscattering spectra from different samples after implantation of a dose of 2 × 10^{16} cm^{-2} of H or D at −120 °C or RT, without any thermal annealing except that taking place when the samples

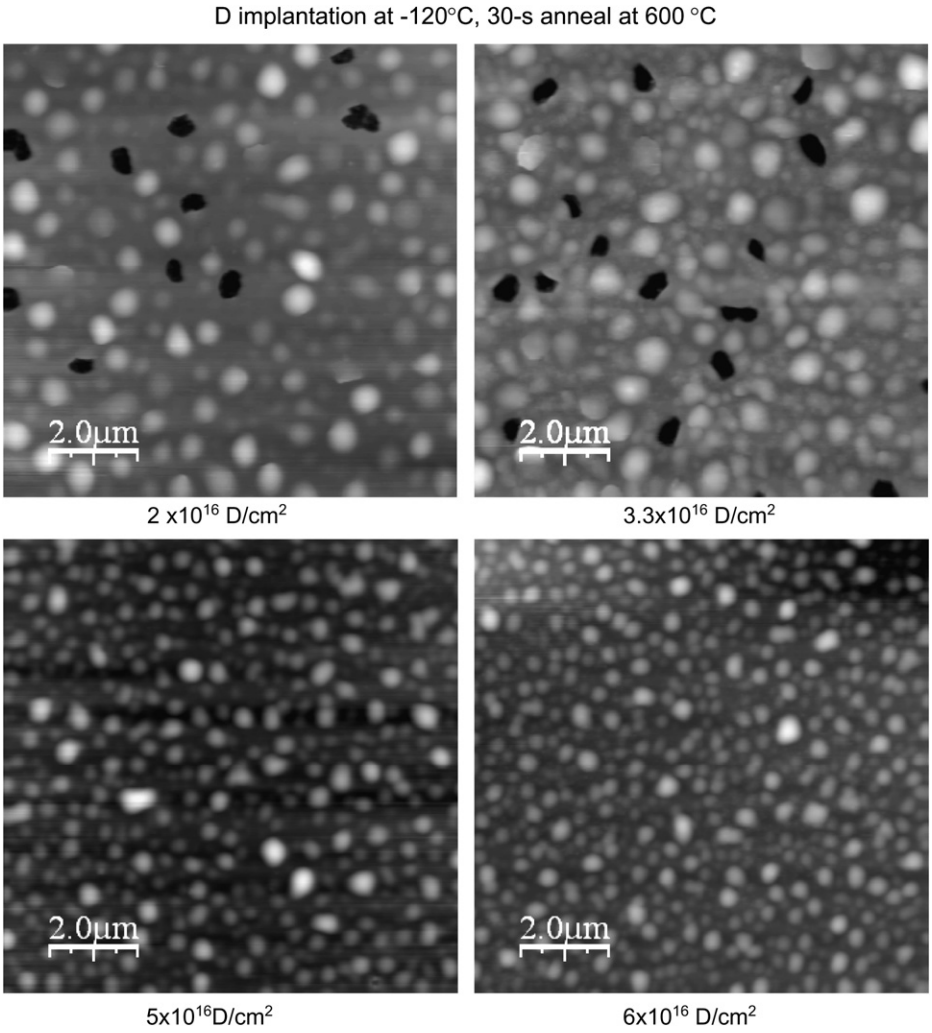

Fig. 1. Atomic force micrographs of the surface of germanium implanted with 5 keV deuterium at −120 °C and rapid thermal annealed at 600 °C; the D atom doses are indicated below each picture.

implanted at LT were brought to RT. The spectra are normalized to the same beam charge to facilitate the comparison. The yield for a virgin sample, also shown, is weak except at the very surface (1.61 MeV), as it should; it is to be compared with the normalized random level (not shown), which is approximately equal to 60 on the same scale. The first feature of the implanted spectra is a peak below the surface at backscattered energies between ~1.53 and ~1.60 MeV. Such a peak is usually considered to be due to atoms displaced from their lattice sites into interstitial positions. Note, however, that the yield of the H-implanted sample is higher than that of the D-implanted sample. This is paradoxical, in terms of atomic collision theory [13], since the primary damage due to D ions is much heavier than that due to H ions because of the higher energy transfer in collisions; for instance the SRIM code [9] predicts the creation of 9.4 vacancy–interstitial (V–I) pairs per incident D ion at 5 keV, compared to 3.0 for H ions. This fact, that the backscattering yield is in no way proportional to the production rate of displaced atoms, indicates that the interactions between the H and D atoms and the created defects, taking place during (dynamic annealing) and after (thermal annealing) implantation, are highly complex (and perplexing). A similar isotope dependence was also observed in Si [14]. It was suggested in that work that a significant part of the backscattering yield–and the dominant part in the case of H – is due to a gross lattice deformation caused by large multivacancies probably containing H_2/D_2 molecules. This hypothesis is further supported by the examination of the depth of the peaks in backscattering. In a first approximation the depth, z, is related to the detected energy, E, by the relation: $z = (kE_0 - E)/(kS_{in} + S_{out}/\cos\theta)$, where $E_0 = 2$ MeV, $k = 0.805$, $S_{in} = 316$ eV/nm, $S_{out} = 337$ eV/nm [9] and $\theta = 10°$. Then the peak for H, at 1.58 MeV, is located 50 nm deep, very close to the H mean range of 54 nm and that for D, at <25 nm, in the region of maximum D damage production [9]. In the case of silicon, the evidence led to the conclusion that the origin of this isotope effect resided in the fact that defect passivation was more effective with H than with D [14]. Thus, the present RBS results would seem to be consistent with this conclusion, but this

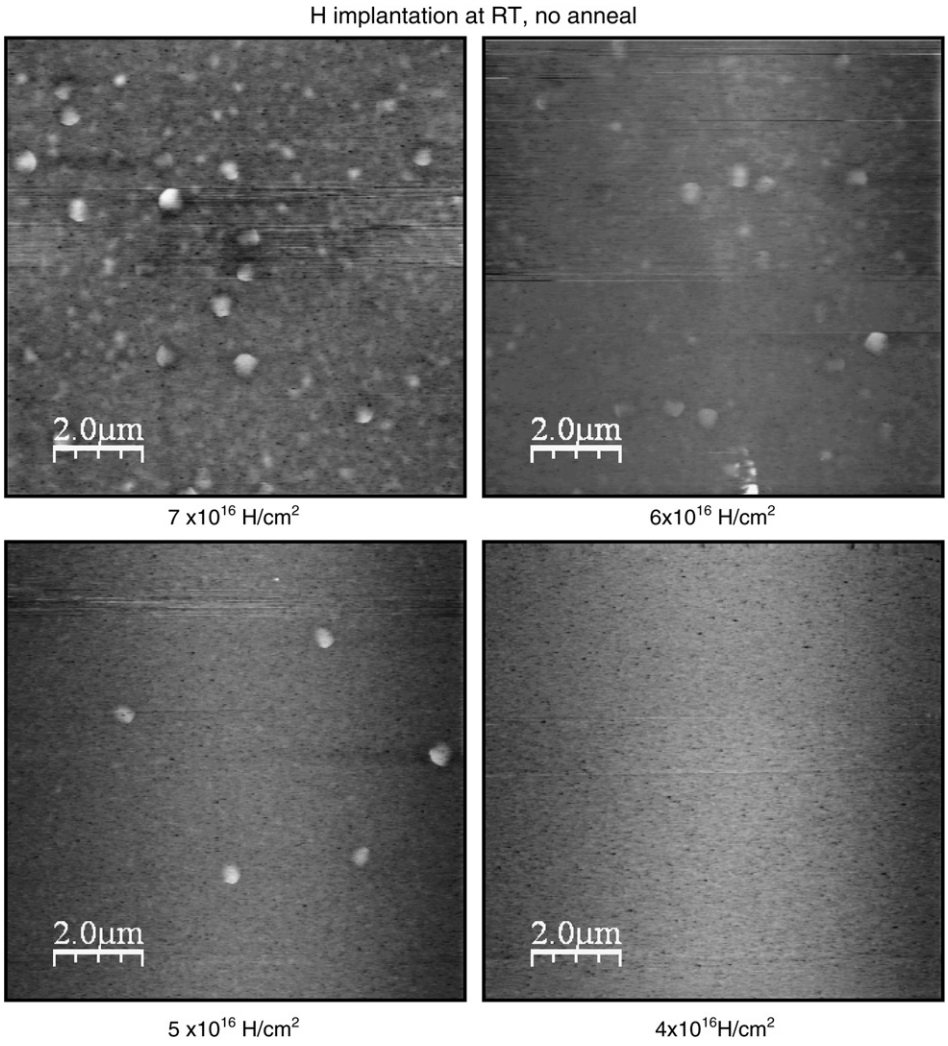

Fig. 2. AFM of Ge after implantation of 5 keV H at RT and no further annealing.

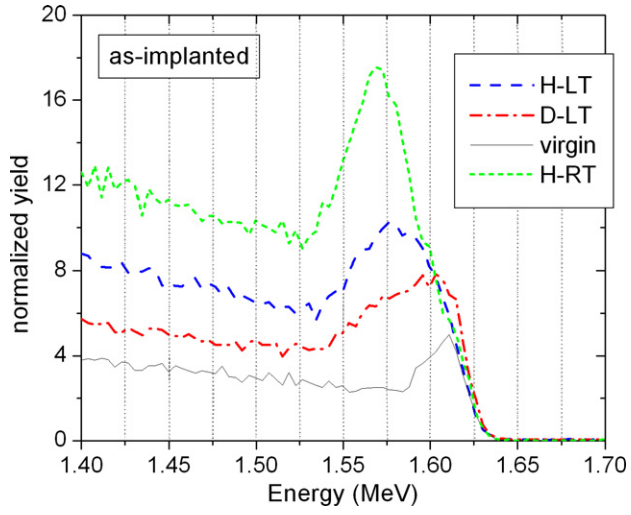

Fig. 3. Rutherford backscattering spectra in the channeling mode for 2×10^{16} cm^{-2} H or D, as-implanted at LT (−120 °C) or RT; the spectrum for a virgin sample is also shown and the random level (not shown) is ~60 on this scale. The spectra are normalized by the beam charge.

will be discussed again later. One can also see in Fig. 3 that, when the H is implanted at RT, the peak is much stronger, sharper and slightly deeper, than at −120 °C. This demonstrates that dynamic annealing during implantation at RT is more effective than purely thermal annealing at RT after implantation at LT to generate whatever defects are responsible for backscattering.

The second feature of the spectra of Fig. 3 is the enhancement in yield beyond the implanted depth ($E <$ 1.53 MeV). This dechanneling is due to the scattering of a fraction of the beam ions at relatively small angles, as a result of which these ions thereafter follow a random trajectory. Dechanneling may be caused by a simple distortion of the lattice, even in the absence of displacements. We see here that the dechanneling yield is roughly proportional to the peak in backscattering, which suggests that it is due to the same defect complexes. It is also interesting to compare the level of dechanneling, D, with the peak in backscattering, P. For definiteness, take the value just beyond the backscattering peak (e.g. at 1.52 MeV for H at RT in

Fig. 3), $D \approx 10$ and compare it to $P \approx 17$; thus $D/P \approx 0.6$. The corresponding ratio at 5 keV in Si [14] is 0.35. At higher energy, it is expected that the dechanneling yield should be relatively stronger, proportionally to the thickness of the damaged layer. This is observed at 100 keV [4] where D/P (Ge) ≈ 1 and D/P (Si) ≈ 0.7. Thus, it appears to be generally true that the relative dechanneling level is stronger in Ge than in Si. It tends to imply that the Ge lattice is more prone to distortion than the Si lattice, in agreement with the mechanical properties.

In Fig. 4 are displayed the backscattering spectra obtained from samples implanted with 2×10^{16} H/cm^2 at RT, either as-implanted or after annealing at 200, 300 and 400 °C. At RT or 200 °C, there is a strong peak centered at 1.57 MeV, corresponding to 67 nm, actually deeper than the mean range of 54 nm. Here it reaches ~30% of the random level. It is to be noted that, in Si, the similar peak reaches only 15–20% of the random level under the same conditions of energy, dose and temperature [14]. This is, again, surprising since the energy transfer by elastic collisions is very ineffective for light ions in the heavier Ge [13]; for instance, the SRIM code [9] predicts 3.0 Ge atom displacements per H ion at 5 keV, compared with 6.8 for Si. This paradox is possibly explained by some observations of Posselt et al. [15], who found that negligible dynamic annealing of defects took place during ion implantation in Ge at RT, contrary to the case of Si.

At 300 °C, a large increase in the displacement yield takes place. This "reverse annealing" also occurs in Si, at roughly the same temperature [14,16]. This phenomenon is not clearly understood, but the evidence [2] is that it is due to hydrogen-related defect structures, possibly tiny H_2-filled cavities [16] and not to an increase in the number of point defects. One can also see that the dechanneling yield increases by about the same factor as the displacement yield. Annealing further up to 400 °C, not only does the backscattering yield increase even more, but the peak widens and shifts to higher energy, i.e. towards the surface. At that temperature the sample is blistered and the very high yield is due in good part, as in the case of Si [17], by the distortion of the surface layer: it is clear that channeling is hardly possible near a surface like that of Fig. 1. Bedell and Lanford [4] also observed this near-surface enhancement when their sample was blistered.

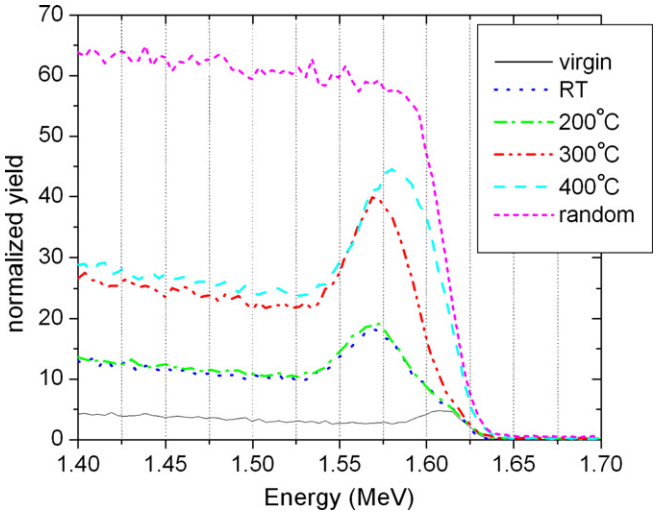

Fig. 4. Rutherford backscattering spectra for Ge implanted at RT with 2×10^{16} H/cm^2 and annealed at the indicated temperatures; the spectrum for a virgin sample and a spectrum taken in a random direction are also displayed.

Thus, the evolution of the kind of defect structures observable by ion channeling appears in several ways similar in Ge as in Si, with the difference that the yield and especially the dechanneling yield, is higher in Ge. It is particularly interesting that a large and puzzling isotope effect is observed as in Si.

3.3. Raman scattering spectroscopy

3.3.1. Medium dose (2×10^{16} cm^{-2})

We show in Fig. 5 the Raman spectra for samples implanted with 2×10^{16} H/cm^2 at LT and annealed at RT, 200 °C and 400 °C; the last is blistered. Three peaks can be distinguished, around 2016, 2048 and 2066 cm^{-1}. In the other comparable study, Zahler et al. [6] observed by infrared absorption (IRA) spectroscopy the same three modes in the wavenumber range $2000 < k < 2050$ cm^{-1}. The slight differences in observed k-values are due to the use of different techniques, because the selection rules are different, the higher frequency mode of a doublet being absent in IRA [18], whereas it can be dominant in RS [19]. Based on the previous work [6] and on the analogy with silicon [19], the mode at 2066 cm^{-1} can be identified with the fully passivated vacancy VH_4 and the one at 2048 cm^{-1} with VH_3 or more probably V_2H_6. The 2016 cm^{-1} mode does not show up at RT; actually one can guess the presence of a shoulder at ~2020 cm^{-1} instead. The 2016 cm^{-1} mode emerges at 200 °C and dominates all others at 400 °C. We therefore attribute the 2016 cm^{-1} mode to Ge-H_2 and/or Ge-H [6] on the (0 0 1)

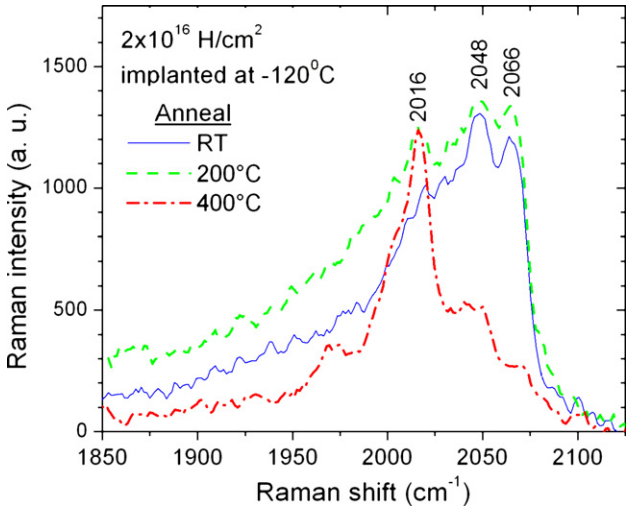

Fig. 5. Raman spectra for 2×10^{16} H/cm^2 implanted at −120 °C and annealed at the indicated temperatures.

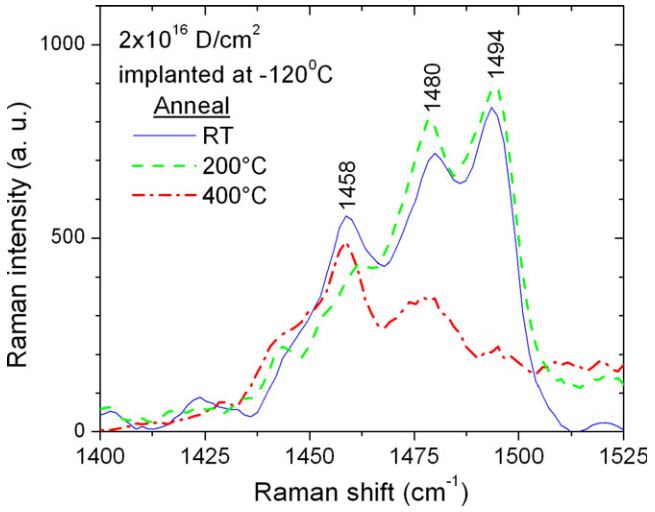

Fig. 6. Raman spectra for 2×10^{16} D/cm^2 implanted at −120 °C and annealed at the indicated temperatures.

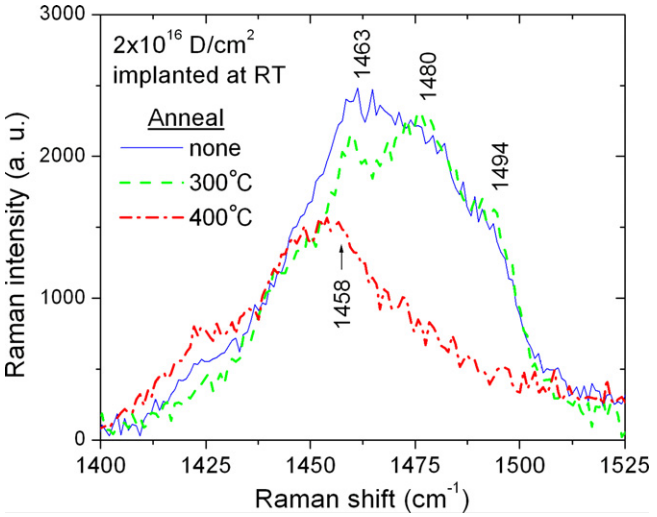

Fig. 7. Raman spectra for 2×10^{16} D/cm^2 implanted at RT and annealed at the indicated temperatures.

internal surfaces of the platelets that are observed by transmission electron microscopy (TEM) [5]. The putative weak mode at ~2020 cm^{-1} could be due to VH_2 [6] or $V_2H_{1,2}$ by analogy with Si [19]. Thus, the thermal evolution of Ge implanted at LT with H ions is characterized by the disappearance of the low frequency modes and also of VH_4, but the persistence of V_2H_6 and finally, the formation of internal surfaces decorated with H_2. This evolution is similar to that of Si implanted at RT [18,19]. Note also that at 200 °C the total amount of Si-bonded H increases above the RT level; this indicates that, after RT implantation, not all H has been captured by dangling bonds yet – and even less so at LT (Fig. 3). It is not known in which form this unbound H is; in the case of Si, at least some of it was detected as H_2 in large multivacancies [14].

Next we discuss D implantation at −120 °C, see Fig. 6. Again three peaks are observed at 1458 cm^{-1} (Ge-D_2), 1480 cm^{-1} (V_2D_6) and 1494 cm^{-1} (VD_4). The *k*-values of these Ge-D stretch modes are all equal to 0.72× those of the corresponding Ge-H modes, in close agreement with the ratio of the square roots of the reduced masses. Actually, these individual peaks appear more prominent than the corresponding Si–H modes in Fig. 5 and the low frequency tail is practically absent. The Ge-D_2 mode does show up at RT, while one at a slightly higher frequency (~1463 cm^{-1}, $V_2D_{1,2}$) makes an appearance at 200 °C. The final outcome is blistering with a strong dominant mode of Ge-D_2 on (0 0 1) together with some V_2D_6. Thus, the thermal evolution of D implanted at −120 °C differs only in details from that of implanted H. This behaviour is in striking contrast with that of D-implanted Si [19], where the low frequency modes do not disappear, the Si–D_2(0 0 1) modes fail to fully develop and the blistering threshold dose is much higher than with H. In Ge, the Raman spectra give no evidence that the vacancies could be less fully passivated with D than with H.

For H or D ions implanted at RT, the spectra are quite different than at −120 °C, as seen in Fig. 7 for D. Now, sharp peaks can no more be found, only a wide enhancement with shoulders. This is the result of the dynamic evolution that has taken place at RT during implantation and we see that the final outcome is different from that obtained with purely thermal evolution at RT following LT implantation (Fig. 6). In Zahler's work [6], the peaks are somewhat more visible, this may be because their samples were actively cooled "at or below RT" during implantation, although the precise temperature is not given. In our as-implanted sample, the spectrum has a maximum at 1463 cm^{-1} (likely VD_2 [6] or $V_2D_{1,2}$, by analogy with Si [19]). At 200 °C, the peaks at ~1460 and 1480 cm^{-1} clearly emerge and finally at 400 °C the internal surfaces and a wide peak centered around ~1455 cm^{-1} dominate. Here, either the mode Ge-D_2 on (0 0 1) is widened by surface imperfections or interaction with neighboring complexes or different complexes are present, such as Ge-D_n, with $n \neq 2$ or on other surfaces than (0 0 1). However, this "fuzziness" in the type of structures present did not impede blistering. Akatsu's TEM work [5] has shown, in addition to platelets, the presence in Ge of spherical cavities with a few nanometer size. The nanocavities appear to form flat clusters in which intercavity fracture leads to microcracking and blistering. The widening of the Raman peak may reflect this diversity in the geometry of the internal surfaces and in the H binding configurations on these surfaces.

3.3.2. *High dose (6×10^{16} H cm^{-2})*

LT implantation of a high dose of 6×10^{16} H/cm^2 results in very heavy radiation damage, even after annealing up to RT. Indeed, the Raman spectrum of Fig. 8 not only shows no sharp peaks, but the usual wide maximum around 2000 cm^{-1} is now accompanied by a twin enhancement around 1900 cm^{-1}. These low-*k* modes may be due to large defect clusters, such as weakly passivated multivacancies, analogous to those identified in silicon [18]. Or else, they may well result from a partial amorphisation of the

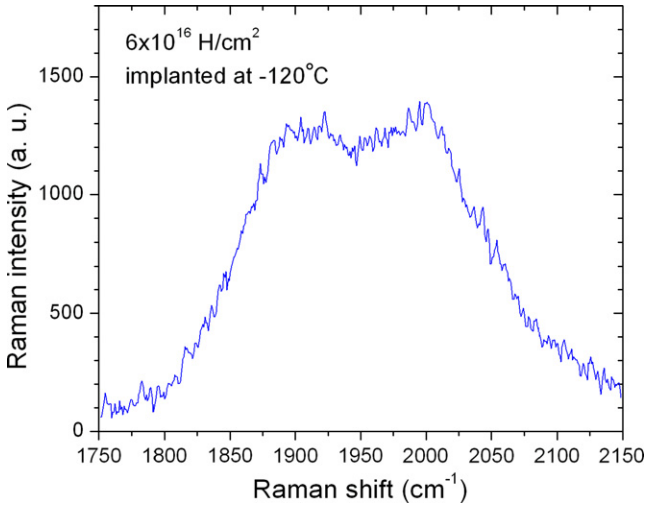

Fig. 8. Raman spectrum for 6×10^{16} H/cm^2 implanted at −120 °C and brought to RT.

sample, since amorphisation will downshift the frequency of vibrational modes. This does not prevent blistering upon annealing. In contrast, if the high H dose is implanted at RT, the dynamic evolution results in a defect structure that is already highly advanced in its evolution towards the formation of hydrogenated internal surfaces and blistering, as exemplified by the Raman spectrum in Fig. 9: The as-implanted sample for 6×10^{16} H cm^{-2} is already dominated by the Ge-H_2 peak at 2016 cm^{-1} – almost similar to that of Fig. 5 for 2×10^{16} cm^{-2} after annealing at 400 °C. And indeed this sample is blistered at RT. After further annealing, some bound H is lost but the spectrum shape does not change. We see here that dynamic evolution during implantation is much more potent than purely thermal annealing in driving the transformation of the defects into large passivated internal surfaces and blistering. The same observation was made in the case of silicon [12].

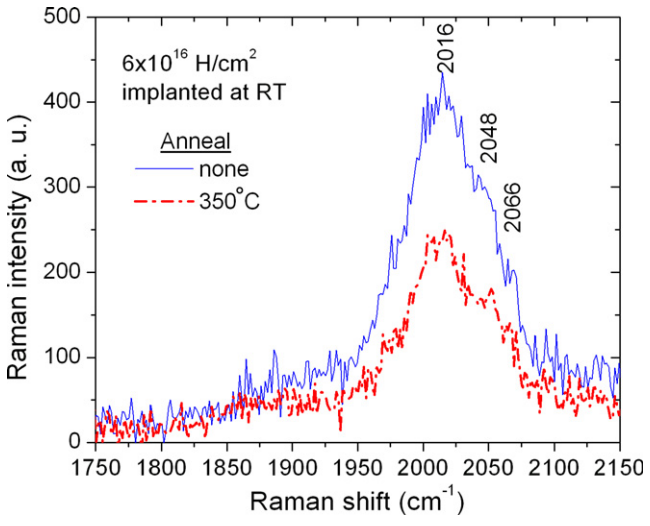

Fig. 9. Raman spectra for 6×10^{16} H/cm^2 implanted at RT and annealed at 350 °C.

4. Discusion and conclusion

The discussion will require that we clearly distinguish between two processes. There is first the purely physical process of "annealing" (dynamic or purely thermal) of point defects and defect clusters (non-passivated), exemplified by the work of Posselt et al. [15] using non reactive heavy Ga^+ projectiles. There is also the physico-chemical "evolution" of hydrogenated complexes into platelets, microcracks and blisters. The point, as we shall see, is that their respective dependences on temperature, material and other parameters are different. Let us recall the main facts.

The evolution of germanium towards blistering (Figs. 1 and 2) is similar to that of silicon at 100–300 °C higher implantation temperature: at a given temperature, the threshold doses are lower than in Si and the isotope effects are almost absent at −120 °C, which only happens at 175 °C in Si.

In contrast, the ion channeling spectra after LT implantation (Fig. 3) show a large isotope effect, as in Si at RT, consistent with a model in which, with H, but not with D, most of the backscattering yield is caused by a lattice deformation due to H- or H_2-containing vacancies. The effect is further increased after RT implantation, due to the dynamic evolution during implantation. In the case of silicon, it was concluded [14] that defect passivation was more effective with H than with D. This was successfully simulated by a lattice kinetic Monte-Carlo computation [20] and could be explained by a simple random walk argument: Since D ions produce ~3× as many point defects as H ions, the D-caused defects have a much higher probability of interacting between themselves (I–V annihilation or I–I and V–V clustering) than interacting with D atoms; in contrast, the simulation indicated that most of the dangling bonds produced by H-irradiation were passivated with H.

However, there is no strong isotope effect in the Raman spectra for Ge (Figs. 5 and 6), consistent with the blistering results. This suggests that, whatever the exact nature of the defects measured by RBS, they are not crucial for blistering, in contrast with the patently essential role of the H-Ge chemistry. This finding is a priori surprising since, in Si, the RBS yield is strongly correlated with the tensile strain normal to the surface, both spatially [21] and as a function of temperature [22,23] and in turn that strain is necessary, in all models [2], for cavity formation and hydrogen absorption into these cavities.

The RBS yield in RT-implanted Ge (Figs. 3 and 4) is much larger than in Si: this is consistent with a slower dynamic annealing of "standard" ("chemically inert") defects in Ge, as in Posselt's work [15], but it is also consistent with a faster dynamic evolution of "hydrogen-related" defects in Ge, since we do know that these complexes cause an increase in the RBS yield called reverse annealing [16] (Fig. 4) under heating.

The Raman spectra of Ge implanted at −120 °C (Figs. 5 or 6) are rather similar to those of Si implanted at RT and

those for Ge implanted at RT (Fig. 7) are similar to those of Si heated up to ~300 °C after RT implantation [19].

High dose implantation in Ge at LT (Fig. 8) gives Raman spectra indicating the presence of amorphisation and/or large defect clusters (low frequency modes), consistent with the weakness of dynamic annealing. In spite of this "handicap", the sample blistered following thermal annealing. High dose implantation at RT shows, in contrast, a terminally evolved defect structure (Fig. 9) and blistering (Fig. 2), consistent with strong dynamic evolution during implantation.

Acknowledgements

This work was supported by the National Science and Engineering Council of Canada and the Fonds Québécois de Recherche sur la Nature et les Technologies.

References

[1] M. Bruel, Electron. Lett. 31 (1995) 1201;
M. Bruel, Nucl. Instr. and Meth. B 108 (1996) 313.
[2] For a review, see B. Terreault, Phys. Stat. Solidi (a) 204 (2007) 2129.
[3] Q.-Y. Tong, K. Gutjahr, S. Hopfe, U. Gösele, T.-H. Lee, Appl. Phys. Lett. 70 (1997) 1390.
[4] S.W. Bedell, W.A. Lanford, J. Appl. Phys. 90 (2001) 1138.
[5] T. Akatsu, K.K. Bourdelle, C. Richtarch, B. Faure, F. Letertre, Appl. Phys. Lett. 86 (2005) 182910.
[6] J.M. Zahler, A. Fontcuberta I Morral, M.J. Griggs, Harry A. Atwater, Y.J. Chabal, Phys. Rev. B 75 (2007) 035309.
[7] M.L. David, F. Pailloux, D. Babonneau, M. Drouet, J.F. Barbot, E. Simoen, C. Claeys, J. Appl. Phys. 102 (2007) 096101.
[8] O. Moutanabbir, A. Giguère, B. Terreault, Appl. Phys. Lett. 84 (2004) 3286.
[9] J.F. Ziegler, J.P. Biersack, SRIM-2003, <www.srim.org>.
[10] I. Horcas, R. Fernandez, J.M. Gomez-Rodriguez, J. Colchero, J. Gomez-Herrero, A.M. Baro, Rev. Sci. Instr. 78 (2007) 013705; Nanotec Electronica <www.nanotec.es>.
[11] A. Giguère, B. Terreault, Surf. Coat. Technol. 201 (2007) 8205.
[12] A. Giguère, B. Terreault, J. Appl. Phys. 102 (2007) 106106.
[13] M.W. Thompson, Defects and Radiation Damage in Metals, Cambridge at the University Press, 1969 (Chapter 4).
[14] O. Moutanabbir, B. Terreault, M. Chicoine, F. Schiettekatte, P.J. Simpson, Phys. Rev. B 75 (2007) 075201.
[15] M. Posselt, L. Bischoff, D. Grambole, F. Herrmann, Appl. Phys. Lett. 89 (2006) 151918.
[16] G.F. Cerofolini, R. Balboni, D. Bisero, F. Corni, S. Frabboni, G. Ottaviani, R. Tonini, R.S. Bruza, A. Zecca, M. Ceschini, G. Giebel, L. Pavesi, Phys. Status Solidi (a) 150 (1995) 539.
[17] R. Tonini, F. Corni, C. Nobili, G. Ottaviani, F. Cazzaniga, G. Queirolo, Solid State Phenom. 82–84 (2002) 291.
[18] M.K. Weldon, V.E. Marsico, Y.J. Chabal, A. Agarwal, D.J. Eaglesham, J. Sapjeta, W.L. Brown, D.C. Jacobson, Y. Caudano, S.B. Christman, E.E. Chaban, J. Vac. Sci. Technol. B 15 (1997) 1065.
[19] O. Moutanabbir, B. Terreault, J. Chem. Phys. 121 (2004) 7973.
[20] T. Zahel, G. Otto, G. Hobler, in: G.K. Celler (Ed.), Electrochem. Soc. Proc. Vol. 2005-03, 2005, p. 79.
[21] M. Nastasi, T. Höchbauer, J.-K. Lee, J.P. Hirth, M. Ridgway, T. Lafford, Appl. Phys. Lett. 86 (2005) 154102.
[22] S. Frabboni, Phys. Rev. B 65 (2002) 165436.
[23] J.-K. Lee, Y. Lin, Q.X. Jia, T. Höchbauer, H.S. Jung, L. Shao, A. Misra, M. Nastasi, Appl. Phys. Lett. 89 (2006) 101901.